Controlling heat ratchet and flow reversal with simple networks

Shuan Wang,[1] Chunhua Zeng,[1,*] Guimei Zhu,[2,†] Hua Wang,[3,‡] and Baowen Li[4]
[1]*Faculty of Science, Kunming University of Science and Technology, Kunming 650500, China*
[2]*School of Microelectronics, Southern University of Science and Technology, Shenzhen 518055, China*
[3]*State Key Laboratory of Complex Nonferrous Metal Resources Clean Utilization, Kunming University of Science and Technology, Kunming 650093, China*
[4]*Department of Materials Science and Engineering and Department of Physics, Southern University of Science and Technology, Shenzhen 518055, China*

(Received 17 April 2023; accepted 11 September 2023; published 4 October 2023)

We investigate ratcheting heat flow in simple networks consisting of a one-dimensional nonlinear chain with a self-coupled loop when the average thermal bias is zero. The effects of coupling strength and temporally averaged environmental reference temperature on the ratcheting heat flow are discussed. It is found that the total heat flow (THF) will be reversed, while heat flow in the self-coupled loop will disappear with the increase of the coupling strength. A critical coupling strength exists at which the THF disappears, and heat flow exists in the self-coupled loop, i.e., eddy ratcheting heat flow displays. The underlining physical mechanisms are analyzed through phonon spectra and unsteady thermal wave dynamics. Furthermore, a reversal of the THF from a negative to a positive value can be controlled by increasing the reference temperature. A critical reference temperature exists at which the negative THF exhibits a maximum value. Phonons dominate the ratcheting heat flow in the self-coupled loop, while solitons dominate the THF for weak coupling strength. These results can possibly be realized in nanoscale experiments and will help to further understand the thermal information on coupled nanotubes, polymer chains, and biological networks.

DOI: 10.1103/PhysRevResearch.5.043009

I. INTRODUCTION

Heat conduction is one of the most fundamental modes of energy transport in nature, finding diverse practical applications. In recent years, significant advancements have been made in this field, yielding a plethora of insightful findings [1–7]. The development of a high-efficiency thermal diode [8] has expanded the scope of thermal research beyond electrons and photons, creating a new area of focus known as phononics [9]. Phononics emphasizes the study of heat transport by vibrational waves in solids, invigorating the traditional field of heat conduction. A microscopic theoretical mechanism for thermal rectification has been proposed by coupling several different materials, where at least one section of the material is nonlinear, based on the principle of resonance and the characteristic of phonon spectra varying with temperature in nonlinear systems [10]. Thermal rectifiers based on this mechanism have been shown to achieve a positive and negative heat flow difference of about twofold, as demonstrated theoretically [11]. With continued research, the rectification ratio may be increased by up to 100 or even 1000 times [12]. The performance of these thermal devices is critically dependent on the properties of the interface between the different materials [13]. In addition, the interface leads to notable alterations in other system properties, such as the tensions at cell-cell interfaces that govern tissue fluidization [14], or the negative energy elasticity resulting from the self-repulsive interface within the lattice polymer chain [15].

The pursuit of thermal diodes continues with ongoing research efforts [16–20]. Furthermore, researchers have proposed other theoretical thermal models, including thermal transistors [21,22], thermal logic gates [23,24], and thermal memory [25]. Moreover, synthetic electric and magnetic fields induce nonreciprocal heat transfer and breakdown of detailed balance [26], generation of phononic frequency combs in driven nonlinear phononic systems through resonances [27], and novel heat conduction formalism reveals distinct types of coherence in thermal phonons [28]. Significant progress has been made not only in theoretical research but also in related experimental work. Examples of recent breakthroughs include thermal rectifiers that deposit heavy molecules on carbon tubes [29], thermal regulators [30], thermal switches [31], and thermal manipulation and rectification in π-stacked organic nanowires [32]. Overall, great strides have been made in the control of phonon transport, i.e., heat flow, both theoretically and experimentally.

The previous works on thermal models mentioned above mainly focus on significant thermal biases, which are difficult to achieve at the nanoscale. However, inspired by Brownian motors [33–37], Ref. [38] proposed a nonbiased, temporally alternating bath temperature to direct *a priori* energy (heat)

*Corresponding author: zchh2009@126.com
†zhugm@sustech.edu.cn
‡wanghua65@163.com

across a spatially extended nonlinear lattice. Once the system is connected to another static heat bath temperature, the system exhibits a vanishing average thermal bias. It is found that the heat ratchet effect exists in a weakly coupled asymmetric Frenkel-Kontorova system. Specifically, when a static temperature gradient exists at both ends of the system, periodic modulation of the heat bath is found to transport heat from the low-temperature end to the high-temperature end, in a direction opposite to the static temperature gradient, resembling the function of a heat pump. Not long after, Ref. [39] found that the Fermi-Pasta-Ulam β (FPU-β) system had a stable directional heat flow in such time-varying heat bath, and the magnitude and direction of heat flow could be tuned by changing the driving frequency.

The relationship between the network and heat conduction has been a subject of recent research interest. For instance, it has been demonstrated that the addition of silicon carbide nanowires to epoxy composites can significantly enhance thermal conductivity, with irregularly arranged nanowires showing the most promising results [40]. In contrast, using silicon carbide particles of similar size and quantity does not yield the same heat conduction improvement. Understanding the underlying mechanisms that govern the heat transfer in such networked systems and identifying more efficient network structures for enhanced heat conduction is an area that requires further investigation. Furthermore, recent studies have utilized cycle flow ranking in network analysis to unveil the fundamental working mechanisms of quantum thermal devices [41]. In the presence of the thermal bias, heat flows spontaneously from a high temperature to a low one, and heat conduction in complex networks have been studied [42–45]. Some interesting works reveal the thermal-siphon phenomenon and thermal/electric conduction for complex networks [44]. Moreover, in polymer chains, drawing amorphous polyethylene reduces self-coupled entanglements, leading to a significant increase in thermal conductivity [46]. In biological networks, such as protein or gene regulatory networks, the presence of self-coupled phenomena holds significance in the transmission and regulation of information [47]. So, for simple networks with a self-coupled loop, a challenging question is whether we can control the ratcheting heat flow by using the coupling interface when the average thermal bias is zero, and if yes, how to do it. In this paper, we shall investigate the ratcheting heat flow in a homogeneous nonlinear system, namely, the self-coupled FPU-β chain that is driven by a one-sided temperature modulated heat bath, as depicted in Fig. 1. By utilizing this time-varying heat bath, the heat conduction behavior in a self-coupled system can be explored without relying on a fixed thermal bias. Our study reveals that the ratcheting heat flow in the self-coupled FPU-β chain can be controlled by adjusting the driving frequency of the time-varying heat bath, the interface coupling strength, etc. Such investigations have significant applications for designing thermal devices in the coupled nanotubes, polymer chains, and biological networks.

II. THE MODEL

We consider the dimensionless Hamiltonian for FPU-β lattice $H = \sum_i [p_i^2/2 + V_i(x_{i+1} - x_i)]$, where $V(x) = x^2/2 + x^4/4$, x_i denotes the displacement, and p_i denotes the momentum from equilibrium position for the ith particle with $i = 1, 2, \ldots, N$. We use fixed boundary conditions $x_0 = x_{N+1} = 0$. The first and last particles, namely, x_1 and x_N, are coupled with the Langevin heat baths, respectively. Therefore, the equation of motion of the system can be expressed as

$$\dot{p}_i = \begin{cases} -\frac{\partial H}{\partial x_i} - \lambda p_i + \xi_i(t), & i = 1, N, \\ -\frac{\partial H}{\partial x_i}, & i = 2, 3, \ldots, N-1, \end{cases} \tag{1}$$

where Gaussian white noise $\langle \xi_{1(N)}(t) \rangle = 0$ and $\langle \xi_{1(N)}(t) \xi_{1(N)}(t') \rangle = 2\lambda k_B T_{L(R)}(t) \delta(t - t')$. $\langle \cdots \rangle$ denotes averaging over noise realizations, the coupling strength between the system and heat bath $\lambda = 1.5$, and the dimensionless Boltzmann constant $k_B = 1$. Symmetry breaking is a well-established prerequisite for achieving a finite directional heat flow. So far, symmetry breaking has primarily been achieved through the introduction of a thermal bias. However, maintaining a significant thermal bias over small distances poses inherent challenges at the nanoscale. In fact, changes in temperature have some periodic behavior on earth, which is caused by a departure from a balance between the incoming and outgoing radiation [48]. To create a system free from thermal bias over extended time averages and induce symmetry breaking, we employ a typical periodic temperature modulation [39]:

$$\begin{aligned} T_L(t) &:= T_L = T_0[1 + A\ \cos(\omega t)], \\ T_R(t) &:= T_R = T_0, \end{aligned} \tag{2}$$

where T_0 is the temporally averaged environmental reference temperature of the system. A and ω are the intensity and driving frequency aid of the thermostat cycle modulation at the left end, respectively. For all of our chosen frequencies ω, the timescale $2\pi/\omega$ of the temperature modulation of the heat bath is much smaller than the timescale to reach local thermal equilibrium. Here the dynamics of the system driven by this heat bath displays a vanishing average thermal bias, i.e.,

$$\overline{\Delta T(t)} \equiv \overline{T_L(t) - T_R(t)} = 0. \tag{3}$$

The time-dependent and asymptotic heat flow $J_i(t)$ corresponds to the periodicity of the external driving period $2\pi/\omega$ after the transients have died out [38]. At these asymptotic long times, the heat flow is equivalent to the average of the

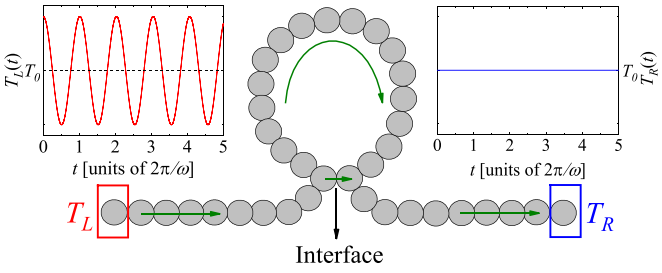

FIG. 1. Schematic setup of a self-coupled FPU-β chain, being coupled to two heat baths at temperatures $T_L(t) := T_L = T_0[1 + A\ \cos(\omega t)]$ and $T_R(t) := T_R = T_0$. The positive direction of heat flow is indicated by the green arrow.

thermal Brownian noise [49],

$$J_i(t) = \left\langle p_i \frac{\partial V}{\partial x_i} \right\rangle. \tag{4}$$

The stationary heat flow $\overline{J}$ then follows as the cycle average over a full temporal period, i.e.,

$$\overline{J(t)} := \overline{J} = \frac{\omega}{2\pi} \int_0^{2\pi/\omega} J_i(t)dt, \tag{5}$$

which becomes independent of particle position i after averaging. Due to the ergodicity being obeyed, this double average equals as well the long-time average

$$\overline{J} = \overline{p_i \partial V/\partial x_i} = \lim_{t\to+\infty} \frac{1}{t} \int_0^t p_i(t)\partial V/\partial x_i|_t dt. \tag{6}$$

It is this heat flow that we generally focus on in our research. Suppose that there is a coupling of strength k between nodes i and j of the chain; then we have an additional new potential $V'_{ij} = k[(x_i - x_j)^2/2 + (x_i - x_j)^4/4]$. The equations of nodes i and j become [50]

$$\dot{p}_i = -\frac{\partial H}{\partial x_i} - \frac{\partial V'_{ij}}{\partial x_i}, \quad \dot{p}_j = -\frac{\partial H}{\partial x_j} - \frac{\partial V'_{ij}}{\partial x_j}. \tag{7}$$

The equations of motion are integrated by the symplectic velocity Verlet algorithm with a small time step $h = 0.005$. The system is simulated at least for a total time $t_{\text{total}} = 10^9$ to allow it to reach a nonequilibrium steady state with local thermal equilibrium, where the local heat flow is constant along the chain. We take the length of the FPU-β lattice as $N = 500$ in the following simulations.

III. THE RESULTS

The two interface particles create a self-coupled loop in the chain, and their coupling position is called the junction. Thus, the heat flow of the system comprises the total heat flow (THF), the heat flow in the self-coupled loop, and the heat flow passing through the interface, denoted by $\overline{J}_T$, $\overline{J}_L$, and $\overline{J}_{\text{int}}$, respectively. This paper investigates the influence of time-varying heat bath and coupling interface on ratcheting heat flow when the temperature of the left heat bath is time varying, and the temperature of the right heat bath is constant. To eliminate the impact of an asymmetric structure on heat flow, we maintain the self-coupled loop equidistant from the left and right heat baths. In Figs. 2–5, we select the junction as $i = 11$, $j = 490$.

With the left and right temperatures exhibiting equality in the long-time average, a pertinent inquiry arises: How can time-varying temperature on the left be manipulated to induce ratcheting heat flow? Furthermore, does the presence of an additional interface impact the conditions under which ratcheting heat flow occurs? In pursuit of answers to these fundamental questions, we first investigate the cycle-averaged ratcheting heat flow $\overline{J}$ as a function of the driving frequency ω (a) and driving strength A (b), as depicted in Fig. 2. In Fig. 2(a), it is evident that when the value of ω surpasses a critical threshold, the left- and right-end particles experience time-averaged constant temperatures, which corresponds to effective thermal equilibrium. Consequently, the heat flows

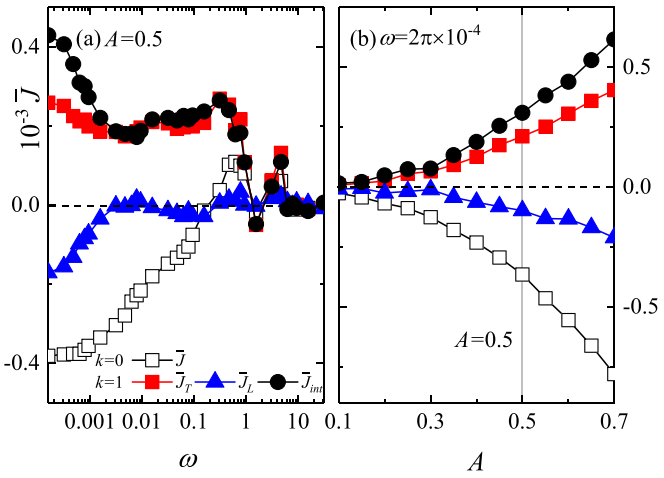

FIG. 2. The cycle-averaged ratcheting heat flow $\overline{J}$ as a function of the driving frequency ω (a) and the driving strength A (b) for the reference temperature $T_0 = 0.5$. The black hollow squares are the heat flow for $k = 0$. The red squares are the total heat flow, the blue triangles are the heat flow in the self-coupled loop, and the black circles are the heat flow going through the interface for $k = 1$. Continuous lines are a guide to the eye.

approach zero with or without coupling. At lower frequencies, the ratcheting heat flow occurs. As expected, it can be seen from Fig. 2(b) that when $A \to 0$, the temperature at both ends is almost equal at all times, which indicates that the system is close to thermal equilibrium, resulting in near-zero heat flows with or without coupling. As the value of A increases, the direction of heat flows remains unchanged, but their magnitude escalates with the increase in A. In short, the generation of ratcheting heat flow necessitates both a sufficiently small frequency and a significant amplitude. Hence we set $\omega = 2\pi \times 10^{-4}$ and $A = 0.5$ below.

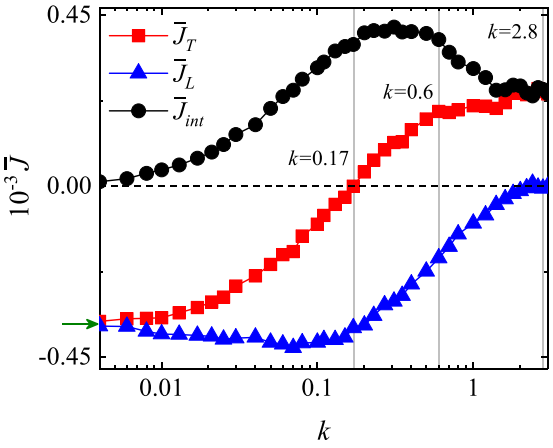

FIG. 3. The cycle-averaged ratcheting heat flow $\overline{J}$ as a function of the coupling strength k for the reference temperature $T_0 = 0.5$, where the red squares are the total heat flow, the blue triangles are the heat flow in the self-coupled loop, and the black circles are the heat flow going through the interface. The green arrow indicates the adiabatic linear transport result derived from Eq. (8), as explained in the text. Continuous lines are a guide to the eye.

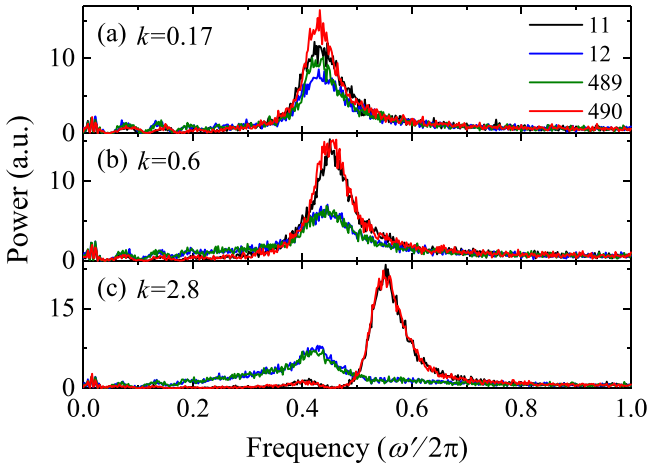

FIG. 4. Phonon spectra of particles 11 (black solid line), 12 (blue solid line), 489 (green solid line), and 490 (red solid line) for $k = 0.17$ (a), $k = 0.6$ (b), and $k = 2.8$ (c). Same parameter values as in Fig. 3.

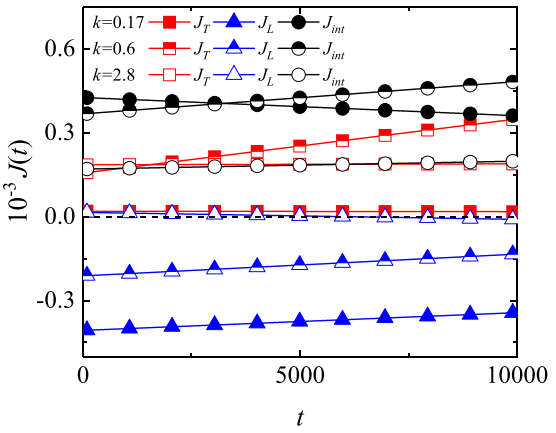

FIG. 5. Fitting of the average value of periodic local heat flow of each particle in the trunk, self-coupled loop, and interface in one cycle of temperature modulation. The line with red squares, blue triangles, and black circles represents J_T, J_L, and $J_{\rm int}$ and the solid, half-solid, and hollow symbols represent $k = 0.17$, $k = 0.6$, and $k = 2.8$, respectively. Same parameter values as in Fig. 3. The figures on the line are just for the eyes to distinguish.

The cycle-averaged ratcheting heat flow $\overline{J}$ as a function of the coupling strength k is depicted in Fig. 3. When considering the limit as $k \to 0$, the influence of the interface becomes negligible. Consequently, $\overline{J}_T \to \overline{J}_L$ and $\overline{J}_{\rm int} \to 0$. Moreover, the slow modulation of temperature allows us to view the periodic effect of dynamic thermal bias as an average, integrated quasistationary flow resulting from the instantaneous static thermal bias. In a linear transport mechanism, this heat flow can be approximated by the linear transport law: $J_i(t) = J_i[\Delta T(t)/N] = \kappa\{[T_L(t) + T_R]/2\}\Delta T(t)/N$. Therefore, in the leading order, the adiabatic net heat flow assumes the following expression [39]:

$$\overline{J_{ad}} = \frac{\omega}{2\pi}\int_0^{2\pi/\omega} \kappa\left[\frac{T_L(t)+T_R}{2}\right]\frac{T_L(t)-T_R}{N}dt$$
$$= \frac{\omega}{2\pi}\int_0^{2\pi/\omega} \kappa\left[T_0 + \frac{AT_0\cos(\omega t)}{2}\right]\frac{AT_0\cos(\omega t)}{N}dt. \quad (8)$$

In the regime of dimensionless temperature $T(t) < 1$, the thermal conductivity of the considered FPU-β lattice exhibits a temperature-dependent behavior, indicated by $\kappa(T) \propto 1/T$ [51,52]. Consequently, the approximate value of $\overline{J_{ad}}$ can be obtained by integrating Eq. (8). This result is indicated by a green arrow in Fig. 3, demonstrating a general agreement with our numerical findings. When the coupling strength is no longer approaching zero, the presence of an additional interface prevents us from theoretically predicting the magnitude of the heat flow *a priori*. Even predicting the direction of the heat flow becomes challenging.

Due to the relatively weak coupling strength ($k < 0.17$), $\overline{J}_L$ exhibits relative stability initially within this region. As the coupling strength further increases, the absolute value of $\overline{J}_L$ gradually decreases until it approaches zero. This behavior can be intuitively understood as the formation of a short-circuit heat flow at the junction under strong coupling, similar to the short-circuit current. It should be noted, without loss of generality, that regardless of the coupling location, $\overline{J}_L$ tends towards zero as the coupling strength becomes relatively large (see Appendix A). The behavior of $\overline{J}_T$ experiences a transition from negative to positive with the gradual increase of coupling strength. Notably, there exists a critical coupling strength ($k = 0.17$) at which $\overline{J}_T$ disappears and heat flow exists solely in the self-coupled loop, namely, the eddy ratcheting heat flow displays; this phenomenon may explain mechanisms of thermal effect for Moore's law in nanodevices. As the value of the coupling strength k continues to increase, $\overline{J}_T$ reaches saturation. Furthermore, our simulation results are consistent with Kirchhoff's first law of heat transfer, where the THF is the sum of the heat flow in the self-coupled loop and the heat flow through the interface, i.e., $\overline{J}_T = \overline{J}_L + \overline{J}_{\rm int}$. In summary, there are three coupling strengths of particular interest: (i) at the critical coupling strength $k = 0.17$, the heat flow through the shortcut rarely flows to the trunk but to the self-coupled loop, resulting in $\overline{J}_T = 0$ and $\overline{J}_L = -\overline{J}_{\rm int}$; (ii) when $k = 0.6$, the results indicate that $\overline{J}_T$ and $\overline{J}_L$ are equal in magnitude and opposite in direction, thus $\overline{J}_{\rm int}$ being twice as much as $\overline{J}_T$ or $-\overline{J}_L$; and (iii) when the coupling strength is very large (e.g., $k = 2.8$), $\overline{J}_L = 0$ and $\overline{J}_T = \overline{J}_{\rm int}$. The coupling strength acts as a switch that not only tunes the magnitudes of the THF, heat flow in the self-coupled loop, and heat flow passing through the interface, but also controls the direction of the THF.

To comprehend the heat ratcheting mechanism at play, we begin by analyzing the phonon spectra of the interface particles for varying coupling strengths of $k = 0.17$, 0.6, and 2.8. This analysis provides us with essential insights into the system's underlying behavior. The phonon spectra of the system are defined as

$$E(\omega') = F(\langle v(t)v(0)\rangle), \quad (9)$$

where $F(\cdots)$ represents Fourier transform and $\langle v(t)v(0)\rangle$ represents the time correlation average of velocity. The match/mismatch of the phonon spectra of the two interface particles controls the ratcheting heat flow. Figure 4 shows the phonon spectra of four particles 11, 12, 489,

and 490 when the system is coupled at the junction $i = 11,\ j = 490$, in which the three coupling strengths mentioned above are taken.

In Fig. 4(a), it can be observed that for $k = 0.17$, the phonon spectra of the four particles are concentrated near 0.42 of frequencies. Notably, the phonon spectra of interface particles 11 and 490 overlaps with the phonon spectra of their neighboring particles 12 and 489 in the self-coupled loop. This indicates that the ratcheting heat flow at the junction is likely to enter the self-coupled loop, which causes the ratcheting heat flow inside the self-coupled loop to increase, and consequently, the THF disappears. In Fig. 4(b), for $k = 0.6$, the phonon spectra of the two interface particles are concentrated near 0.45 of frequencies. However, the phonon spectra of their neighboring particles 12 and 489 are concentrated near 0.42, implying a decrease in the overlap. As a result, the ratcheting heat flow inside the self-coupled loop decreases, leading to an increase in the THF. Finally, at $k = 2.8$, Fig. 4(c) displays a mismatch between the phonon spectra of the interface particles and their neighbors. The phonon spectra of interface particles 11 and 490 are concentrated near 0.5, while the phonon spectra of their neighboring particles 12 and 489 are still concentrated near 0.42. This causes the ratcheting heat flow to exit the self-coupled loop and not reenter it, resulting in a zero ratcheting heat flow inside the self-coupled loop and a maximum THF. In a word, with the increase of coupling strength, the phonon spectra matching degree of the two interface particles gradually becomes higher, while the phonon spectra matching degree between interface particles and the neighboring particles in the self-coupled loop gradually becomes lower, which leads to the gradual decrease of $\overline{J}_L$, while $\overline{J}_T$ gradually becomes larger, until the phonon spectra are completely mismatched and $\overline{J}_L = 0$, thus maximizing $\overline{J}_T$. To further understand the variations of the THF, the heat flow in the self-coupled loop, and the heat flow passing through the interface, we analyze the unsteady thermal wave dynamics of the ratcheting heat flow. In one period $[t \in (0, 2\pi/\omega)]$, the average of the periodic local heat flow is

$$J_{T/L/\mathrm{int}}(t) = \frac{1}{n_{T/L/\mathrm{int}} n_1} \sum_{i}^{n_{T/L/\mathrm{int}}} \sum_{j}^{n_1} J_i(t + 2j\pi/\omega), \qquad (10)$$

where $n_{T/L/\mathrm{int}}$ represents the total number of heat flows passing through the trunk, inner self-coupled loop, and interface, and n_1 is the number of periods. We recorded data points every $t = 100$ in one cycle, then averaged the data over 50 000 cycles for each point. The resulting values were then fitted to obtain the magnitude of the ratcheting heat flow, as shown in Fig. 5.

From Fig. 5, it is apparent that within one period, the behavior of the THF, the heat flow in the self-coupled loop, and the heat flow passing through the interface change with the increase of the coupling strength. When $k = 0.17$, the THF is close to zero, while the heat flow in the self-coupled loop is always negative. Simultaneously, the heat flow passing through the interface is always positive, and its value is almost equal to the negative heat flow through the self-coupled loop. When $k = 0.6$, the THF is always positive, while the heat flow in the self-coupled loop is always negative, and their average values are almost symmetrical about $J(t) = 0$. The heat flow passing through the interface is always positive, equal to the THF minus the heat flow in the self-coupled loop. When $k = 2.8$, the THF is always positive, while the heat flow in the self-coupled loop is close to zero. Furthermore, the heat flow passing through the interface almost coincides with the THF. These results are consistent with the behavior of the ratcheting heat flow depicted in Fig. 3.

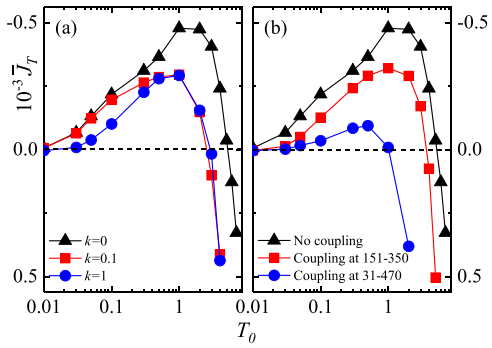

FIG. 6. The cycle-averaged ratcheting heat flow $\overline{J}_T$ as a function of the reference temperature T_0. (a) Coupling at $i = 91,\ j = 410$ for $k = 0$ (black triangles), $k = 0.1$ (red squares), and $k = 1$ (blue circles); (b) no coupling (black triangles), coupling at $i = 151,\ j = 350$ (red squares), and $i = 31,\ j = 470$ (blue circles) for $k = 1$. Continuous lines are a guide to the eye.

Next, we are further interested in how the THF is affected by the reference temperature in simple networks. The reference temperature present in the system can induce maximum and reversal of the THF. The cycle-averaged ratcheting heat flow $\overline{J}_T$ as a function of the reference temperature T_0 is depicted in Fig. 6. We observe a reversal of the THF from a negative to a positive value with increasing T_0. When the THF is negative, the THF first increases to a maximum and then decreases with the increase of T_0, which corresponds to a critical reference temperature that exists at which the negative THF exhibits a maximum. Simultaneously, for a small value of weak coupling strength ($k = 0.1$), the height of the maximum is decreased, and the position of the maximum is unaltered compared with no coupling ($k = 0$). As the value of the coupling strength continues increasing ($k = 1$), the height and position of the maximum are almost unchanged, which means that the critical reference temperature is not sensitive to the coupling strength. But as the value of self-coupled length is increased, the height of the maximum is decreased, and the position of the maximum is changed to small values of T_0, which means that the critical reference temperature is sensitive to the self-coupled length. However, when the THF is positive, the positive THF increases with the increase of T_0. Similarly, in the case of $k = 0$ (no coupling), where the system has no extra interface, it can be approximately described by the linear transport law. Equation (8) is reformulated as

$$\overline{J_{ad}} = \frac{\omega}{2\pi} \int_0^{\pi/\omega} \frac{AT_0 \sin(\omega t)}{N} \left\{ \kappa \left[T_0 + \frac{AT_0 \sin(\omega t)}{2} \right] - \kappa \left[T_0 - \frac{AT_0 \sin(\omega t)}{2} \right] \right\} dt. \qquad (11)$$

At low temperatures, the heat conductivity exhibits a proportionality to $\kappa \propto 1/T$ due to the weak coupling limit, while at high temperatures, the heat conductivity follows a

scaling behavior of $\kappa \propto T^{1/4}$, which can be understood from the perspective of scaling arguments [51,52]. Specifically, with a low or high T_0, the expression $\kappa[T_0 + AT_0 \sin(\omega t)/2]$ is consistently lower or higher, respectively, than $\kappa[T_0 - AT_0 \sin(\omega t)/2]$ within the time window of $[0, \pi/\omega]$. Consequently, the ratcheting heat flow undergoes a transition from negative to positive as T_0 increases. This prediction is demonstrated to agree with our numerical calculations in Fig. 6. It is noteworthy that when T_0 is less than 0.01, the ratcheting heat flow remains negative but approaches zero due to the extremely small value of T_0.

According to the above results, the interface particles play a significant role in influencing both the THF and the heat flow in the self-coupled loop. By changing the potential energy of the interface particles, we found that the phonon dominates the ratcheting heat flow in the self-coupled loop, and the soliton dominates the THF for weak coupling strength. For details, see Appendix B.

IV. CONCLUSIONS AND DISCUSSIONS

In this paper, we investigate the ratcheting heat flow in simple networks consisting of a one-dimensional nonlinear chain with a self-coupled loop. We keep the self-coupled loop equidistant from the left and right heat baths, in which the temperature of the left heat bath is time varying and the temperature of the right heat bath is constant. The effects of coupling strength and temporally averaged environmental reference temperature on the ratcheting heat flow are discussed, respectively. When the system is coupled at the junction $i = 11$, $j = 490$, the absolute value of the heat flow in the self-coupled loop gradually decreases until it is almost close to zero with the gradual increase of coupling strength. The behavior of the THF experiences a transition from negative to positive with the increase of coupling strength. There exists a critical coupling strength where the THF disappears and heat flow exists in the self-coupled loop, namely, the eddy ratcheting heat flow displays. The THF reaches saturation as the coupling strength continues increasing. The underlining heat ratcheting mechanisms are analyzed by the phonon spectra of the interface particles and the unsteady thermal wave dynamics of the ratcheting heat flow. We show a reversal of the THF from a negative to a positive value with increasing reference temperature. When the THF is negative, the THF first increases, reaches a maximum, and then decreases with the increasing of the reference temperature, which corresponds to a critical reference temperature that exists at which the negative THF exhibits a maximum. The critical reference temperature is sensitive to the self-coupled length by comparison with the coupling strength. For weak coupling strength, the phonon dominates the ratcheting heat flow in the self-coupled loop, and the soliton dominates the THF. In addition, the findings of effective temperature distribution support the behavior of ratcheting heat flow (see Appendix C).

Self-coupling phenomena are commonly observed in polymer chains and biological networks, making them practical examples for studying these effects [53]. When self-coupling occurs, a coupling interface is added to the system, and an appropriate coupling strength may lead to the eddy heat flow. To date, controlling heat flow has mainly depended on manipulating temperature gradients, with the system producing different thermal conductivity or rectification rates through heterogeneous structures. However, it is challenging to maintain a significant temperature gradient over short distances at the nanoscale [54]. By generating ratcheting heat flow through heat baths with an average zero thermal bias, we were able to use a dimensionless ambient reference temperature that falls within the controllable temperature range of laboratory experiments [49]. Moreover, homogeneous structures are easier to prepare, more programmable, and reusable compared to heterogeneous structures. Therefore, using a time-varying temperature heat bath to manipulate heat flow and transfer heat information by altering temperature, coupling position, and strength is more feasible. We are optimistic that our results, such as the eddy ratcheting heat flow, can be understood mechanisms of thermal effect for Moore's law in nanodevices and look forward to seeing their practical implementation.

ACKNOWLEDGMENTS

This work was supported by the National Natural Science Foundation of China (Grants No. 12265017 and No. 12247205), Yunnan Fundamental Research Projects (Grants No. 202201AV070003 and No. 202101AS070018), Yunnan Province Ten Thousand Talents Plan Young and Elite Talents Project, and Yunnan Province Computational Physics and Applied Science and Technology Innovation Team. The authors thank P. Ao and Z. Liu for valuable comments and insightful discussions.

APPENDIX A: DIFFERENT COUPLING POSITIONS

In this section, the cycle-averaged ratcheting heat flow $\overline{J}$ as a function of the coupling strength k for the coupling at $i = 11$, $j = 490$ (a), $i = 21$, $j = 480$ (b), $i = 31$, $j = 470$ (c), and $i = 151$, $j = 350$ (d) is shown in Fig. 7. The findings demonstrate that as the coupling strength increases, the

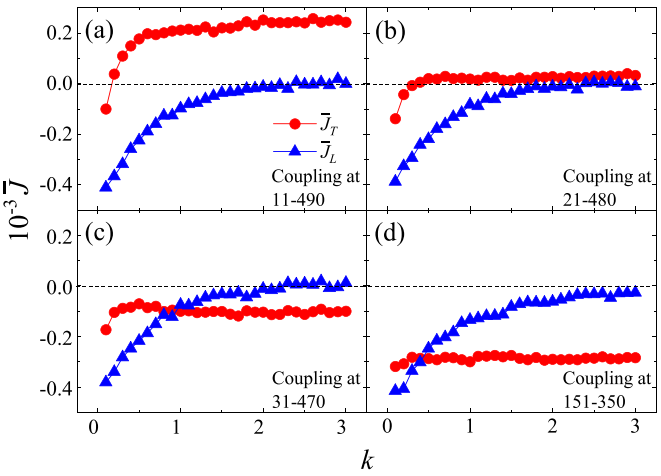

FIG. 7. The-cycle averaged ratcheting heat flow $\overline{J}$ as a function of the coupling strength k for the coupling at $i = 11$, $j = 490$ (a), $i = 21$, $j = 480$ (b), $i = 31$, $j = 470$ (c), and $i = 151$, $j = 350$ (d). The red circles are the total heat flow and the blue triangles are the heat flow in the loop. Same T_0, A, and ω values as in Fig. 3. Continuous lines are a guide to the eye.

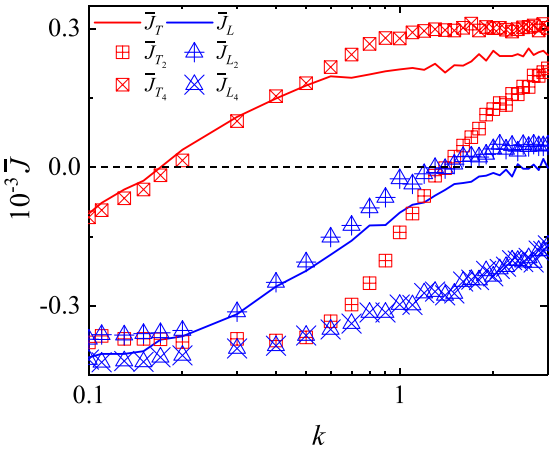

FIG. 8. The cycle-averaged ratcheting heat flow $\overline{J}$ as a function of the coupling strength k, where the red solid line and squares are the total heat flow, and the blue solid line triangles are the heat flow in the self-coupled loop. The cross represents harmonic coupling, and the × represents nonlinear coupling. The $\overline{J}_T$ and $\overline{J}_L$ corresponding to the solid line are consistent with Fig. 3. Same coupling position and T_0, A, and ω values as in Fig. 3.

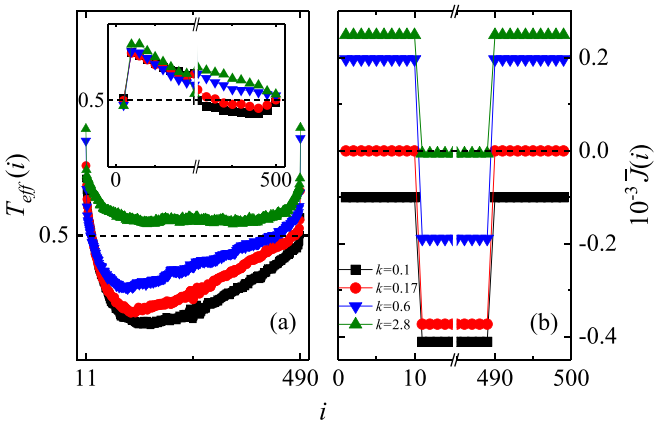

FIG. 9. Effective temperature distribution $T_{\rm eff}(i)$ for the self-coupled loop (a) and the outer part of the loop (inset) and the cycle-averaged ratcheting heat flow distribution $\overline{J}(i)$ (b) for $k = 0.1$ (black squares), $k = 0.17$ (red circles), $k = 0.6$ (blue triangles), and $k = 2.8$ (green inverted triangles). Same coupling position and T_0, A, and ω values as in Fig. 3. Continuous lines are a guide to the eye.

heat flow in the self-coupled loop gradually decreases until it stabilizes at zero. Notably, the THF gradually moves in a positive direction when the two coupling particles are weakly coupled ($k < 1$), whereas it remains relatively stable when the coupling strength is strong ($k > 1$). Furthermore, the analysis indicates that the THF gradually moves in a negative direction as the self-coupled loop length decreases. Note that only when the coupling loop is long, as discussed in the text, will the THF disappear or reverse as the coupling strength increases.

APPENDIX B: DIFFERENT COUPLING POTENTIALS

When the two particles are coupled by harmonic terms, only phonons can pass smoothly, whereas when the two particles are coupled only by nonlinear terms, only solitons can pass through smoothly due to the phonon vacuum effect [55–58]. Thus an interesting question is, how do the harmonic or nonlinear terms in the interface-coupled potential affect the THF and heat flow in the self-coupled loop? To answer this question, we assume the three different coupling potentials

$$V'_{ij} = \begin{cases} k[(x_i - x_j)^2/2 + (x_i - x_j)^4/4], \\ k(x_i - x_j)^2/2, \\ k(x_i - x_j)^4/4. \end{cases} \tag{B1}$$

The THF and heat flow in the self-coupled loop as a function of the coupling strength k is shown in Fig. 8. When the two particles are coupled with harmonic potential, for weak coupling strength ($k < 1$), the change trend of $\overline{J}_{L_2}$ is consistent with the behavior of $\overline{J}_L$, and $\overline{J}_{T_2}$ is far from $\overline{J}_T$. When the two particles are coupled with a quartic potential, for weak coupling strength ($k < 1$), the change trend of $\overline{J}_{T_4}$ is consistent with the behavior of $\overline{J}_T$, and $\overline{J}_{L_4}$ is far from $\overline{J}_L$. That is, the phonon dominates the ratcheting heat flow in the self-coupled loop, and the soliton dominates the THF for weak coupling strength.

APPENDIX C: THE EFFECTIVE TEMPERATURE AND RATCHETING HEAT FLOW DISTRIBUTIONS

To further understand the ratcheting heat flow in simple networks consisting of a one-dimensional nonlinear chain with a self-coupled loop when the average thermal bias is zero, we need to go to the definition of effective temperature. In computer simulations, it is more convenient to compute the averages of kinetic energy by following a single trajectory over time. This is often referred to as the time average, which can be expressed as [39]

$$T_{\rm eff}(i) = \lim_{N_t \to \infty} \frac{\sum_{t=1}^{N_t} p_i^2(t)}{N_t} = \overline{p_i^2}. \tag{C1}$$

The temperature is a measure of the kinetics of the particle, i.e., it is an ensemble (time) average of the kinetic energy. Without coupling, the middle particle at a chain is connected only by its two nearest neighbors. After coupling, the middle particle is connected with three particles which change its equation of motion. This introduces not only an interface thermal resistance at the junction but also a junction to the transfer of energy. We plot the effective temperature and ratcheting heat flow distributions with different coupling strength k in Fig. 9. There is always a temperature jump at the end particle linked to the time-varying heat bath which is shown in Fig. 9(a). When the chain is self-coupled together, regardless of k, there is also a temperature jump at the junction and the coupled particles have roughly the same temperature. With increasing k, the temperature of the majority of the self-coupled loop progressively rises from below the reference temperature to approximate it. Correspondingly, the temperature of the outer part of the loop, which is linked to one side of the thermostatic heat bath, increases from below the reference temperature to above it. These changes in

temperature are reflected in the magnitude and direction of the heat flow. As shown in Fig. 9(b), when k increases, we can see that the heat flow in the self-coupled loop is negative, and its absolute value decreases to zero gradually. The THF experiences a reversal from negative to positive with the increase of k. There exists a critical coupling strength $k = 0.17$ where THF disappears and heat flow exists in the self-coupled loop.

[1] S. Lepri, R. Livi, and A. Politi, Heat conduction in chains of nonlinear oscillators, Phys. Rev. Lett. **78**, 1896 (1997).

[2] T. Prosen and D. K. Campbell, Momentum conservation implies anomalous energy transport in 1D classical lattices, Phys. Rev. Lett. **84**, 2857 (2000).

[3] A. Dhar, Heat conduction in a one-dimensional gas of elastically colliding particles of unequal masses, Phys. Rev. Lett. **86**, 3554 (2001).

[4] P. L. Garrido, I. P. Hurtado, and B. Nadrowski, Simple one-dimensional model of heat conduction which obeys Fourier's law, Phys. Rev. Lett. **86**, 5486 (2001).

[5] B. Li, H. Zhao, and B. Hu, Can disorder induce a finite thermal conductivity in 1D lattices? Phys. Rev. Lett. **86**, 63 (2001).

[6] B. Li, L. Wang, and B. Hu, Finite thermal conductivity in 1D models having zero Lyapunov exponents, Phys. Rev. Lett. **88**, 223901 (2002).

[7] S. Lepri, R. Livi, and A. Politi, Thermal conduction in classical low-dimensional lattices, Phys. Rep. **377**, 1 (2003).

[8] B. Li, L. Wang, and G. Casati, Thermal diode: Rectification of heat flux, Phys. Rev. Lett. **93**, 184301 (2004).

[9] L. Wang and B. Li, Phononics gets hot, Phys. World. **21**, 27 (2008).

[10] C. Starr, The copper oxide rectifier, J. Appl. Phys. **7**, 15 (1936).

[11] M. Terraneo, M. Peyrard, and G. Casati, Controlling the energy flow in nonlinear lattices: A model for a thermal rectifier, Phys. Rev. Lett. **88**, 094302 (2002).

[12] B. Li, J. Lan, and L. Wang, Interface thermal resistance between dissimilar anharmonic lattices, Phys. Rev. Lett. **95**, 104302 (2005).

[13] B. Hu, L. Yang, and Y. Zhang, Asymmetric heat conduction in nonlinear lattices, Phys. Rev. Lett. **97**, 124302 (2006).

[14] S. Kim, M. Pochitaloff, G. A. Stooke-Vaughan, and O. Campàs, Embryonic tissues as active foams, Nat. Phys. **17**, 859 (2021).

[15] N. C. Shirai and N. Sakumichi, Solvent-induced negative energetic elasticity in a lattice polymer chain, Phys. Rev. Lett. **130**, 148101 (2023).

[16] L. Defaveri and C. Anteneodo, Analytical results for a minimalist thermal diode, Phys. Rev. E **104**, 014106 (2021).

[17] M. Romero-Bastida and M. Lindero-Hernández, Thermal rectification in three-dimensional mass-graded anharmonic oscillator lattices, Phys. Rev. E **104**, 044135 (2021).

[18] Y. Li, J. Li, M. Qi, C. W. Qiu, and H. Chen, Diffusive nonreciprocity and thermal diode, Phys. Rev. B **103**, 014307 (2021).

[19] N. Kalantar, B. K. Agarwalla, and D. Segal, Harmonic chains and the thermal diode effect, Phys. Rev. E **103**, 052130 (2021).

[20] T. J. Shimokusu, Q. Zhu, N. Rivera, and G. Wehmeyer, Time-periodic thermal rectification in heterojunction thermal diodes, Int. J. Heat Mass Transfer **182**, 122035 (2022).

[21] B. Li, L. Wang, and G. Casati, Negative differential thermal resistance and thermal transistor, Appl. Phys. Lett. **88**, 143501 (2006).

[22] N. Gupt, S. Bhattacharyya, B. Das, S. Datta, V. Mukherjee, and A. Ghosh, Floquet quantum thermal transistor, Phys. Rev. E **106**, 024110 (2022).

[23] L. Wang and B. Li, Thermal logic gates: Computation with phonons, Phys. Rev. Lett. **99**, 177208 (2007).

[24] A. Hamed, M. Elzouka, and S. Ndao, Thermal calculator, Int. J. Heat Mass Transfer **134**, 359 (2019).

[25] L. Wang and B. Li, Thermal logic gates: Computation with phonons, Phys. Rev. Lett. **101**, 267203 (2008).

[26] S.-A. Biehs and G. S. Agarwal, Breakdown of detailed balance for thermal radiation by synthetic fields, Phys. Rev. Lett. **130**, 110401 (2023).

[27] L. Cao, D. Qi, R. Peng, M. Wang, and P. Schmelcher, Phononic frequency combs through nonlinear resonances, Phys. Rev. Lett. **112**, 075505 (2014).

[28] Z. Zhang, Y. Guo, M. Bescond, J. Chen, M. Nomura, and S. Volz, Heat conduction theory including phonon coherence, Phys. Rev. Lett. **128**, 015901 (2022).

[29] W. Chang, D. Okawa, H. Garcia, A. Majumdar, and A. Zettl, Solid-state thermal rectifier, Science **314**, 1121 (2006).

[30] E. Langenberg, D. Saha, M. E. Holtz, J. J. Wang, D. Bugallo, E. Ferreiro-Vila, H. Paik, I. Hanke, S. Ganschow, D. A. Muller, L. Q. Chen, G. Catalan, N. Domingo, J. Malen, D. G. Schlom, and F. Rivadulla, Ferroelectric domain walls in $PbTiO_3$ are effective regulators of heat flow at room temperature, Nano Lett. **19**, 7901 (2019).

[31] T. Du, Z. Xiong, L. Delgado, W. Liao, J. Peoples, R. Kantharaj, P. R. Chowdhury, A. Marconnet, and X. Ruan, Wide range continuously tunable and fast thermal switching based on compressible graphene composite foams, Nat. Commun. **12**, 4915 (2021).

[32] B. Liu, Y. Chen, and X. Xu, Thermal manipulation and thermal rectification in π-stacked organic nanowires, Nanoscale **13**, 13641 (2021).

[33] P. Reimann, R. Bartussek, R. Häussler, and P. Hänggi, Brownian motors driven by temperature oscillations, Phys. Lett. A **215**, 26 (1996).

[34] P. Reimann and P. Hänggi, Introduction to the physics of Brownian motors, Appl. Phys. A **75**, 169 (2002).

[35] P. Reimann, Brownian motors: Noisy transport far from equilibrium, Phys. Rep. **361**, 57 (2002).

[36] P. Hänggi, F. Marchesoni, and F. Nori, Brownian motors, Ann. Phys. **517**, 7 (2005).

[37] P. Hänggi and F. Marchesoni, Artificial Brownian motors: Controlling transport on the nanoscale, Rev. Mod. Phys. **81**, 387 (2009).

[38] N. Li, P. Hänggi, and B. Li, Ratcheting heat flux against a thermal bias, Europhys. Lett. **84**, 40009 (2008).

[39] N. Li, F. Zhan, P. Hänggi, and B. Li, Shuttling heat across one-dimensional homogenous nonlinear lattices with a Brownian heat motor, Phys. Rev. E **80**, 011125 (2009).

[40] D. Shen, Z. Zhan, Z. Liu, Y. Cao, L. Zhou, Y. Liu, W. Dai, K. Nishimura, C. Li, C. T. Lin, N. Jiang, and J. Yu, Enhanced thermal conductivity of epoxy composites filled with silicon carbide nanowires, Sci. Rep. **7**, 2606 (2017).

[41] L. Wang, Z. Wang, C. Wang, and J. Ren, Cycle flux ranking of network analysis in quantum thermal devices, Phys. Rev. Lett. **128**, 067701 (2022).

[42] K. Xiong, C. Zeng, Z. Liu, and B. Li, Influence of the degree of a complex network on heat conduction, Phys. Rev. E **98**, 022115 (2018).

[43] K. Xiong, J. Zhou, M. Tang, C. Zeng, and Z. Liu, Control of thermal conduction and rectification in a model of complex networks with two asymmetric parts, Phys. Rev. E **98**, 062144 (2018).

[44] K. Xiong, Z. Liu, C. Zeng, and B. Li, Thermal-siphon phenomenon and thermal/electric conduction in complex networks, Natl. Sci. Rev. **7**, 270 (2020).

[45] K. Xiong, Z. Yan, Y. Xie, and Z. Liu, Regulating heat conduction of complex networks by distributed nodes masses, Sci. Rep. **11**, 5501 (2021).

[46] R. Shrestha, P. Li, B. Chatterjee, T. Zheng, X. Wu, Z. Liu, T. Luo, S. Choi, K. Hippalgaonkar, M. P. D. Boer, and S. Shen, Crystalline polymer nanofibers with ultra-high strength and thermal conductivity, Nat. Commun. **9**, 1664 (2018).

[47] G. Karlebach and R. Shamir, Modelling and analysis of gene regulatory networks, Nat. Rev. Mol. Cell Biol. **9**, 770 (2008).

[48] R. Benzi, G. Parisi, A. Sutera, and A. Vulpiani, A theory of stochastic resonance in climatic change, SIAM J. Appl. Math. **43**, 565 (1983).

[49] B. Hu, B. Li, and H. Zhao, Heat conduction in one-dimensional chains, Phys. Rev. E **57**, 2992 (1998).

[50] Z. Liu and B. Li, Heat conduction in simple networks: The effect of interchain coupling, Phys. Rev. E **76**, 051118 (2007).

[51] K. Aoki and D. Kusnezov, Fermi-Pasta-Ulam β Model: Boundary jumps, Fourier's law, and scaling, Phys. Rev. Lett. **86**, 4029 (2001).

[52] N. Li and B. Li, Temperature dependence of thermal conductivity in 1D nonlinear lattices, Europhys. Lett. **78**, 34001 (2007).

[53] S. Dorogovtsev and J. Mendes, Evolution of networks, Adv. Phys. **51**, 1079 (2002).

[54] J. Ren and B. Li, Emergence and control of heat current from strict zero thermal bias, Phys. Rev. E **81**, 021111 (2010).

[55] G. D. Mahan, Traveling solitons in one-dimensional quartic lattices, Phys. Rev. B **74**, 094304 (2006).

[56] S. Neogi and G. D. Mahan, Generation of traveling solitons in one-dimensional monatomic quartic lattices, Phys. Rev. B **78**, 064306 (2008).

[57] S. Sen and T. R. K. Mohan, Dynamics of metastable breathers in nonlinear chains in acoustic vacuum, Phys. Rev. E **79**, 036603 (2009).

[58] E. Ávalos, D. Sun, R. L. Doney, and S. Sen, Sustained strong fluctuations in a nonlinear chain at acoustic vacuum: Beyond equilibrium, Phys. Rev. E **84**, 046610 (2011).